applied sciences

MDPI

Article

Influence Analysis of a Higher-Order CSI Effect on AMD Systems and Its Time-Varying Delay Compensation Using a Guaranteed Cost Control Algorithm

Chaojun Chen [1], Zuohua Li [1,*], Jun Teng [1,*] and Ying Wang [2]

[1] School of Civil and Environment Engineering, Shenzhen Graduate School, Harbin Institute of Technology, Shenzhen 518055, Guangdong, China; chenchaojun@stmail.hitsz.edu.cn

[2] Department of Civil and Environmental Engineering, University of Surrey, Guildford GU2 7XH, UK; ying.wang@surrey.ac.uk

* Correspondence: lizuohua@hit.edu.cn (Z.L.); tengj@hit.edu.cn (J.T.); Tel.: +86-755-2603-4949 (Z.L.)

Academic Editor: César M. A. Vasques
Received: 12 February 2017; Accepted: 20 March 2017; Published: 23 March 2017

Abstract: A control-structure interaction (CSI) effect commonly exists between an active mass damper/driver (AMD) system with a DC motor and a controlled building. Additionally, its higher-order component leads to the fact that the actual control force acts behind its theoretical time; i.e., time delay. In this paper, the main influencing factors of a higher-order CSI effect are analyzed, including the input frequency of the control voltage, the structural parametric uncertainties, and the control gains. In addition, a new time-delay compensation controller based on a guaranteed cost control (GCC) algorithm is designed, to consider the higher-order CSI effect for multi-level steel frame structures. Experiments on a typical four-storey frame are conducted, to verify the performances of the proposed method. The results show that the proposed controller has an excellent control effect and stable control parameters, even under the situation of large parametric uncertainties and long time-varying delays.

Keywords: vibration control; active mass damper/driver; control-structure interaction; time-varying delay; guaranteed cost control

1. Introduction

A passive tuned mass damper (TMD) [1–3] and active mass damper/driver (AMD) [4–6] are used to control the dynamic response of highly flexible buildings that are horizontally situated under a strong load, e.g., wind and earthquake. Indeed, the application of TMD is more extensive than AMD. Theoretically, the performance of an AMD control system is better than other forms of systems [7]. However, the negative influence of time-delay, which results in performance degradation and even in the instability of the system, limits its development and practical application [8,9].

A time-delay effect mainly stems from the actuator response, which is primarily caused by a Control-Structure Interaction (CSI) effect, which exists between any type of structural active control system and its target structures. Therefore, the influence of the CSI effect on an AMD control system should be carefully considered when designing such a system [10–13]. The actuator response time-delay is due to negative phases existing in the transfer function from control voltage to control force, but the influence of the frequency of control voltage on its phase (corresponding to actuator response time-delay) has often been neglected. Obviously, the actuator response time-delay induced by the CSI effect is affected by the sensitivity of the actuators, which is largely dependent on the drive mode. An electromagnetic drive is one of the most common forms in AMD control systems [14,15],

and the influence of the CSI effect on such systems needs to be focused on. In addition to these above references, the research on the CSI effect mainly concentrates on its influence on the control effect of control systems [16–18], or the impact of the CSI effect on structural dynamics [19]. Indeed, the structural dynamics are coupled with the performance of an AMD system with a CSI effect, and its performance is mainly connected with control gains. Meanwhile, different dynamical behaviors of civil engineering structures may result from structural parametric uncertainties [20]. However, the influences of control gains and uncertainties on the CSI effect remain unknown. In order to achieve a higher performance of an AMD system with a CSI effect, it is necessary to investigate the influencing factors of the CSI effect, including the input frequencies of control voltage, structural parametric uncertainties, and control gains.

After analyzing such factors, several measures can be obtained to reduce this effect. In addition, to further solve the CSI problem, a suitable compensation control strategy is needed. Firstly, a Linear Quadratic Regulator (LQR) is a common control strategy for high-rise buildings [21], but it requires an accurate mathematical model. As a parameter perturbation or time-varying delay exists in a control system using LQR, its expected performance and stability are difficult to guarantee [22]. At present, the Linear Matrix Inequality (LMI) [23] approach is widely applied to analyze the stability of time-delay systems [24,25] or design a H∞ time-delay compensation controller [26,27]. However, H∞ control mainly considers the robust stability of the system by sacrificing its performance. To overcome this difficulty, a Guaranteed Cost Control (GCC) algorithm is proposed as a special LQR control method [28,29]. In order to successfully apply the GCC algorithm for a high-rise building with an AMD control system, a key step involves solving a positive-definite solution of Riccati matrix equations. Previously, this problem has been based on the Riccati equation method, whose convergence cannot be guaranteed [30,31]. However, an LMI approach can overcome this difficulty [32]. Several above References [10–13] also indicate that classical algorithms cannot be effectively applied to eliminate the negative influence of a higher-order CSI effect. Therefore, in view of the structural parametric uncertainties and time-varying delays caused by a higher-order CSI effect, a new time-delay compensation controller is needed. This paper proposes the combination of a GCC algorithm and an LMI approach, to enhance the performance and robustness of the AMD system, which is different from those in the above references and is of great significance for civil engineering.

In this paper, a mathematical model of the higher-order CSI effect is established for a multi-storey steel frame with its AMD control system. The influences of the input frequencies of control voltage, structural parameters, and control gains on a higher-order CSI effect, are analyzed. A new time-delay compensation method based on a GGC algorithm and LMI approach is proposed for time-varying delay systems with uncertain structural parameters. Numerical experiments are conducted on a four-storey frame with its AMD control system. Further, the numerical model has been constructed in the laboratory. Discussions and conclusions that are conducted to verify the performances of the proposed method are presented based on both numerical and experimental results.

2. Experimental Model Considering CSI Effect

2.1. Time-Delay Sources of a Control System

According to the work flow of an AMD control system, the time-delay shown in Figure 1 mainly results from: (1) Structural response d_1; (2) Sensors monitoring d_2; (3) Feedback signals are transmitted from the sensors to the controller d_3; (4) Control force calculation d_4; (5) Control signals are transmitted from the controller to the actuator d_5; and (6) Actuator response d_6. The minimal delays (d_3 and d_5) of the transmission of signals in wires can be ignored, in terms of the delays (d_1, d_2, and d_4) that are basically unchanged. In this paper, the actuator response time-delay d_6 constitutes the important research content.

An AMD control system that considers the CSI effect can be described in Figure 2. v, u, and w are the control voltage, control force, and external excitation load, respectively. H_{vy} denotes the transfer

function from the structural response to the control voltage, H_{uv} denotes the transfer function from the control voltage to the control force, and H_{yu} denotes the transfer function from the control force and the external excitation load to the structural response. A CSI effect occurs at the stage of H_{uv}.

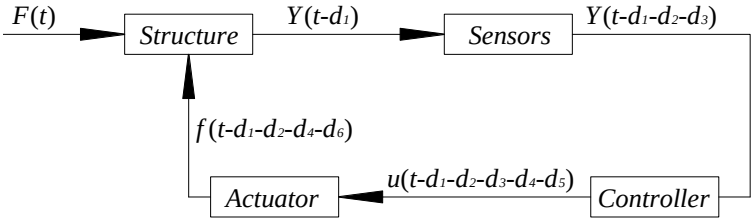

Figure 1. Model of an AMD control system.

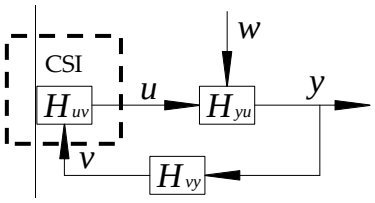

Figure 2. A Flow diagram of an AMD control system showing CSI.

2.2. Experimental System and Its Theoretical Model

The experimental model shown in Figure 3 is a four-storey shearing type structure made of steel [6]. The columns and the floors of the test structure are made of two thin steel plates, which are 8 mm thick and 30 mm width. The length of the floors is 1400 mm, and the interstory height of the structure is 800 mm.

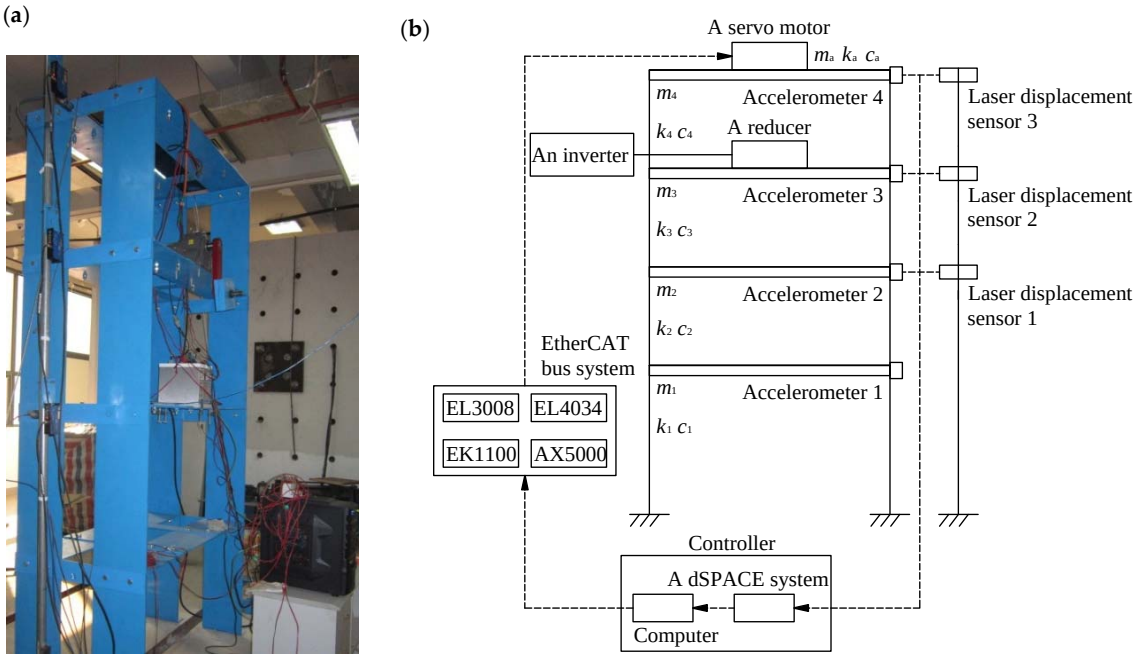

Figure 3. Pictures of the steel frame structure, (**a**) Practicality; (**b**) Exhibition.

In this experiment, four accelerometers are installed in the beam-column joints of each structural floor to measure the structural response, respectively. Accelerometers with a type of GT02 and

three Micro-Epsilon laser displacement sensors are used to measure the horizontal acceleration and displacement of each floor, along the minor-axis. Here, the acceleration measurement is used as the feedback signal to calculate the real-time control forces, and then, an EtherCAT bus system can be used for transmitting the forces to a servo motor. The displacement measurement of the second, third, and fourth floors are used for verifying the control effectiveness. The loading system is composed of a reducer with an eccentric mass and an inverter. The frequency range of the inverter is 0–50 Hz, and the speed range is 0–120 rpm. The AMD control system shown in Figure 3b mainly includes a servo motor from a local company, an EtherCAT bus system, a dSPACE with a type of DS1103, and a computer. During the tests, the chassis of the AMD control device is fixed on the fourth floor of the structure and all of the motion signals are gathered by the dSPACE. An EL3008 input terminal, an EK1100 coupling terminal, an EL4034 output terminal, and a servo controller with a type of AX5000 constitute the EtherCAT bus system, which can be used to ensure the accuracy of signal transmission.

After calculating, its structural frequencies are listed in Table 1.

Table 1. Natural frequencies of the experimental system.

Order	Frequency (Hz)
1	0.162
2	0.589
3	1.093
4	1.852

Regarding the simplified model of the experimental system, as shown in Figure 4, the control force is exerted on the top floor. Therefore, the force equilibrium of the control system is:

$$M\ddot{X}(t) + C\dot{X}(t) + KX(t) = B_{gs}\ddot{x}_g(t) + B_s u(t) \quad (1)$$

where M, C, and K are the mass matrix, damping matrix, and stiffness matrix of the system, respectively. $\ddot{X}$, $\dot{X}$, and X are the acceleration, velocity, and displacement vectors of the system relative to the ground, respectively. $\ddot{x_g}$ is the external excitation. B_s and B_{gs} are the position matrices of the control force and earthquake, respectively. u is the active, controllable magnetic force of the AMD system.

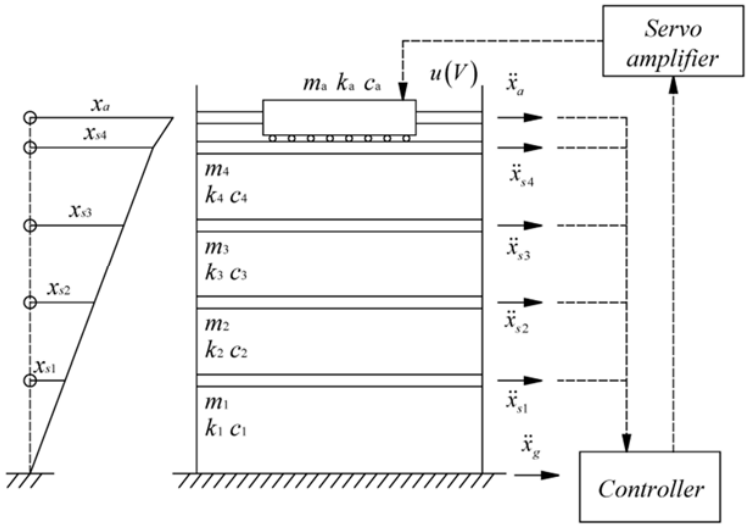

Figure 4. The simplified model of an AMD system.

The experimental structure is modeled as an in-plane lumped-mass shear structure, and the matrices M, C, K, X, B_s, and B_{gs} are expressed as:

$$M = \begin{bmatrix} m_1 & 0 & 0 & 0 & 0 \\ 0 & m_2 & 0 & 0 & 0 \\ 0 & 0 & m_3 & 0 & 0 \\ 0 & 0 & 0 & m_4 & 0 \\ 0 & 0 & 0 & 0 & m_{\mathrm{a}} \end{bmatrix}_{5\times5}, C = \begin{bmatrix} c_1+c_2 & -c_2 & 0 & 0 & 0 \\ -c_2 & c_2+c_3 & -c_3 & 0 & 0 \\ 0 & -c_3 & c_3+c_4 & -c_4 & 0 \\ 0 & 0 & -c_4 & c_4+c_a & -c_a \\ 0 & 0 & 0 & -c_a & c_a \end{bmatrix}_{5\times5},$$
$$K = \begin{bmatrix} k_1+k_2 & -k_2 & 0 & 0 & 0 \\ -k_2 & k_2+k_3 & -k_3 & 0 & 0 \\ 0 & -k_3 & k_3+k_4 & -k_4 & 0 \\ 0 & 0 & -k_4 & k_4+k_a & -k_a \\ 0 & 0 & 0 & -k_a & k_a \end{bmatrix}_{5\times5}, X = \begin{bmatrix} x_{s1} \\ x_{s2} \\ x_{s3} \\ x_{s4} \\ x_a \end{bmatrix}_{5\times1}, B_s = \begin{bmatrix} 0 \\ 0 \\ 0 \\ -1 \\ 1 \end{bmatrix}_{5\times1}, B_{gs} = -M[1]_{5\times1}. \quad (2)$$

where x_{si} are the relative displacements of the ith floor and x_a is the relative displacement of the AMD. m_a, c_a, and k_a are the mass, damping, and stiffness of the AMD, respectively. m_i, k_i, and c_i are the mass, interstorey stiffness, and damping of the ith floor, respectively.

The state vector of the system, which includes the displacement and velocity, is $Z = [X\ \dot{X}]^T$, so Equation (1) can be expressed as the state-space equation, as follows:

$$\dot{Z}(t) = AZ(t) + B_1\ddot{x}_g(t) + B_2u(t) \quad (3)$$

where A, B_1, and B_2 are the state matrix, the excitation matrix, and the control matrix, respectively, which can be expressed as:

$$A = \begin{bmatrix} 0_{5\times5} & I_{5\times5} \\ -M^{-1}K & -M^{-1}C \end{bmatrix}, B_1 = \begin{bmatrix} 0_{5\times1} \\ M^{-1}B_{gs} \end{bmatrix}, B_2 = \begin{bmatrix} 0_{5\times1} \\ M^{-1}B_s \end{bmatrix} \quad (4)$$

2.3. CSI Effect Analysis

This section analyzes the essence of the CSI effect of an AMD control system with a DC motor, shown in Figure 5. It is modeled as a permanent magnet DC motor that is usually used in the control field of civil structures. Because there is a natural feedback path between the structure and the actuator, the CSI effect is unavoidable and needs to be considered [13]. Since the AMD mass is embedded with magnetic coil sets, the input-output relationship of a DC motor that allows for a concise analysis is:

$$\dot{T}(t) = -\frac{R_a}{L_a}T(t) - \frac{K_bK_iK_g}{L_ar_m}\dot{x}_A(t) + \frac{K_i}{L_a}V(t) \quad (5)$$

where T is the motor torque, V is the applied voltage, L_a = 0.00073 H is the armature inductance, R_a = 0.0099 Ω is the armature resistance, K_b = 1.27 V/s is the back electromotive force constant, K_i = 1.2 Nm/A is the motor torque constant, and K_g = 1 and r_m = 0.15 m are the gear ratio and the lead of the ball screw, respectively.

The absolute velocity of the AMD is:

$$\dot{x}_A = \dot{x}_a - \dot{x}_{s4} \quad (6)$$

where $\dot{x}_{s4}$ and $\dot{x}_a$ are the relative velocities of the fourth floor and the AMD.

The horizontal control force produced by the rotary motor with its ball-screw can be defined as:

$$u(t) = \frac{K_g}{r_m}T(t) \quad (7)$$

Figure 5. A photograph of the DC motor.

An equation for the force and its transform can be obtained by substituting Equation (6) into Equation (5).

$$\dot{u}(t) = -\frac{R_a}{L_a}u(t) - \frac{K_b K_i K_g^2}{L_a r_m^2}\dot{x}_A(t) + \frac{K_i K_g}{L_a r_m}V(t) \tag{8}$$

Then:

$$u(t) = -\frac{L_a}{R_a}\dot{u}(t) - \frac{K_b K_i K_g^2}{R_a r_m^2}\dot{x}_A(t) + \frac{K_i K_g}{R_a r_m}V(t) \tag{9}$$

where $-K_b K_i K_g^2 \dot{x}_A / R_a r_m^2$ and $-L_a \dot{u} / R_a$ are the control force loss caused by the reverse induction voltage and the inductance of the motor coils, respectively.

The AMD is regarded as an analysis object, and the control force can be written as:

$$u = m_a \ddot{x}_A + c_a \dot{x}_A + k_a x_A \tag{10}$$

By using the Laplace transform, Equation (10) can be written as:

$$u = s^2 m_a x_A + s c_a x_A + k_a x_A \tag{11}$$

The absolute displacements x_A of the AMD is:

$$x_A = \frac{u}{s^2 m_a + s c_a + k_a} \tag{12}$$

As can be seen from Equations (9) and (12), there is an additional variable (relative structural velocity of the fourth floor) in Equation (9), meaning that the dynamical property of the AMD control system is coupled with the structural dynamics. Furthermore, a first-order differential of force also exists in Equation (9). As a result, corresponding to the different accuracy requirements of the solution, three models with different CSI effects can be established. Thus, Figure 6 is a block diagram representation of the different AMD models given in Equations (9) and (12).

Regarding the DC motor installed on the example frame, three models can be shown in Figure 6: (1) Non-CSI effect only contains the item (a); (2) Considering the reduced-order CSI effect, the items (a) and (b) are contained, and the higher-order item (c) is neglected; (3) Considering the higher-order CSI effect, the items (a–c) are all considered. Different transfer functions from the control voltage to the control force are shown in Figures 7 and 8.

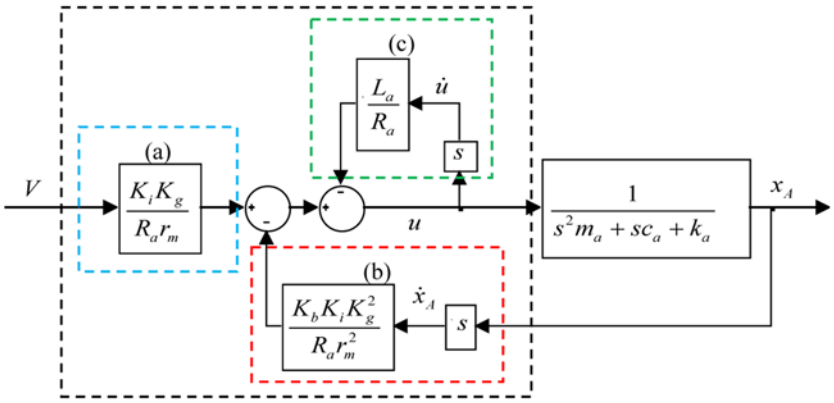

Figure 6. Block diagram of three CSI models.

2.3.1. Non-CSI Effect

In this case, the AMD control system can be regarded as an ideal linear actuator, and the relationship between the control force and voltage is:

$$u = \frac{K_iK_g}{R_ar_m}V \tag{13}$$

The state equation of this system is:

$$\dot{Z} = \begin{bmatrix} 0 & I \\ -\frac{K}{M} & -\frac{C}{M} \end{bmatrix} Z + \begin{bmatrix} 0 \\ \frac{B_s}{M} \end{bmatrix} \frac{K_iK_g}{R_ar_m}V + \begin{bmatrix} 0 \\ \frac{B_{gs}}{M} \end{bmatrix} \ddot{x}_g \tag{14}$$

The observation equation is:

$$Y = \begin{bmatrix} I & 0 \\ 0 & I \\ -\frac{K}{M} & -\frac{C}{M} \\ 0 & 0 \end{bmatrix} Z + \begin{bmatrix} 0 \\ 0 \\ \frac{B_s}{M} \\ 1 \end{bmatrix} \frac{K_iK_g}{R_ar_m}V + \begin{bmatrix} 0 \\ 0 \\ \frac{B_{gs}}{M} \\ 0 \end{bmatrix} \ddot{x}_g \tag{15}$$

Since the relationship between the control force and control voltage is linear, the magnitude of the transfer function is a constant. A non-CSI effect is considered, which means that the phase of the transfer function is zero and the control force maintains the same phase with the control voltage, resulting in a transformation process that does not contain a time-delay.

2.3.2. Considering Reduced-Order CSI Effect

In this case, the differential term of the control force is neglecting, namely $-(L_a/R_a)\dot{u} = 0$. Then, the relationship between the input and output of the DC motor is:

$$u = \frac{-K_bK_iK_g^2}{R_ar_m^2}\dot{x}_A + \frac{K_iK_g}{R_ar_m}V \tag{16}$$

The state equation of this system is:

$$\begin{aligned}\dot{Z} &= \begin{bmatrix} 0 & I \\ -\frac{K}{M} & -\frac{C}{M} \end{bmatrix} Z + \begin{bmatrix} 0 \\ \frac{B_s}{M} \end{bmatrix} \left(-\frac{K_b K_i K_g^2}{R_a r_m^2} \right) \dot{x}_A + \begin{bmatrix} 0 \\ \frac{B_s}{M} \end{bmatrix} \frac{K_i K_g}{R_a r_m} V + \begin{bmatrix} 0 \\ \frac{B_{gs}}{M} \end{bmatrix} \ddot{x}_g \\ &= \left(\begin{bmatrix} 0 & I \\ -\frac{K}{M} & -\frac{C}{M} \end{bmatrix} + \frac{K_b K_i K_g^2}{R_a r_m^2} \begin{bmatrix} 0 \\ \frac{B_s}{M} \end{bmatrix} \begin{bmatrix} 0 & B_s^T \end{bmatrix} \right) Z + \begin{bmatrix} 0 \\ \frac{B_s}{M} \end{bmatrix} \frac{K_i K_g}{R_a r_m} V + \begin{bmatrix} 0 \\ \frac{B_{gs}}{M} \end{bmatrix} \ddot{x}_g \end{aligned} \tag{17}$$

The observation equation is:

$$Y = \left(\begin{bmatrix} I & 0 \\ 0 & I \\ -\frac{K}{M} & -\frac{C}{M} \\ 0 & 0 \end{bmatrix} + \frac{K_b K_i K_g^2}{R_a r_m^2} \begin{bmatrix} 0 \\ 0 \\ \frac{B_s}{M} \\ 1 \end{bmatrix} \begin{bmatrix} 0 & B_s^T \end{bmatrix} \right) Z + \begin{bmatrix} 0 & 0 \\ 0 & 0 \\ \frac{B_{gs}}{M} & \frac{K_i K_g}{R_a r_m} \frac{B_s}{M} \\ 0 & \frac{K_i K_g}{R_a r_m} \end{bmatrix} \begin{bmatrix} \ddot{x}_g \\ V \end{bmatrix} \tag{18}$$

From Figure 7, with the increase of frequency, the magnitude of the transfer function becomes larger, before tending to a definite value. The phase transforms from a minus value to zero; a minus phase indicates that a control force lags behind control voltage. Therefore, the time-delay of the control voltage to the control force gradually reduces to zero, with the increasing frequency of the control voltage. The nonlinear relationship between the control force and control voltage is influenced by the changing frequency of the control voltage (or feedback signal), which is consistent with Equation (17). Additionally, as the frequency of the control voltage is consistent with the natural frequency of the experimental frame, a sudden change in the transfer function is generated.

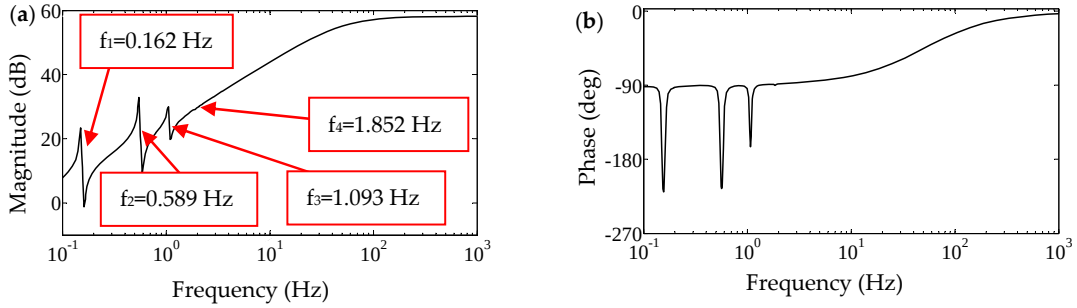

Figure 7. Transfer function from control voltage to control force (Reduced-order CSI effect), (**a**) Magnitude; (**b**) Phase.

2.3.3. Considering Higher-Order CSI Effect

In this case, the relationship between the input and output of the DC motor is:

$$u = -\frac{L_a}{R_a} \dot{u} - \frac{K_b K_i K_g^2}{R_a r_m^2} \dot{x}_A + \frac{K_i K_g}{R_a r_m} V \tag{19}$$

The state equation of this system is:

$$\dot{\hat{Z}} = \begin{bmatrix} 0 & I & 0 \\ -\frac{K}{M} & -\frac{C}{M} & \frac{B_s}{M} \\ 0 & \frac{K_b K_i K_g^2}{L_a r_m^2} B_s^T & -\frac{R_a}{L_a} \end{bmatrix} \hat{Z} + \begin{bmatrix} 0 & 0 \\ \frac{B_{gs}}{M} & 0 \\ 0 & \frac{K_i K_g}{L_a r_m} \end{bmatrix} \begin{bmatrix} \ddot{x}_g \\ V \end{bmatrix} \tag{20}$$

where $\hat{Z} = \begin{bmatrix} X & \dot{X} & u \end{bmatrix}^T$. The observation equation is:

$$Y = \begin{bmatrix} I & 0 & 0 \\ 0 & I & 0 \\ -\frac{K}{M} & -\frac{C}{M} & \frac{B_s}{M} \\ 0 & 0 & 1 \end{bmatrix} \hat{Z} + \begin{bmatrix} 0 & 0 \\ 0 & 0 \\ \frac{B_{gs}}{M} & 0 \\ 0 & 0 \end{bmatrix} \begin{bmatrix} \ddot{x}_g \\ V \end{bmatrix} \tag{21}$$

From Figure 8, with the increasing frequency of the control voltage, the magnitude and phase of the transfer function initially increase and then decrease. This phenomenon indicates that a long time-delay exists when the frequency is relatively large or small.

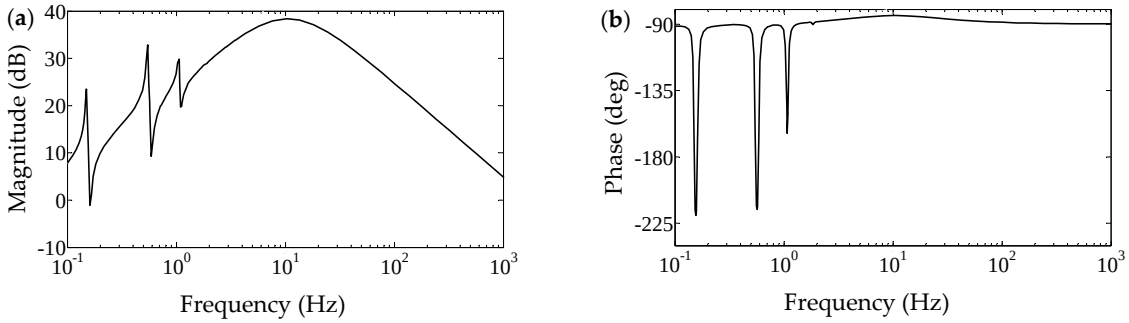

Figure 8. Transfer function from control voltage to control force (Higher-order CSI effect), (**a**) Magnitude; (**b**) Phase.

From Figures 7 and 8, as the AMD system does not consider the CSI effect, the control force generated by a unit control voltage is the largest, and the time-delay is close to zero. This means that the performance of the servo motor without the CSI effect is preferable to that of the reduced-order CSI effect, and the worst performance is seen by the higher-order CSI effect. When the worst condition occurs, system time-delay always exists (negative phases), and the frequency of the control voltage needs to be decreased or increased properly to near the value which is located at the peak of the magnitude and phase curves. Finally, in order to obtain the largest magnitude and the smallest phase, the frequency of the experimental system is taken as 10 Hz. An influence analysis of the frequency on the magnitude of the transfer function from the control voltage to the control force can be found in much literature. However, the basic conception of its negative influence on the phase has been introduced here. In sum, as a suitable frequency of the control voltage is selected, a unit control voltage can be converted into a relatively large control force, and the additional time-delay is relatively short.

The influence of external disturbance on an AMD system can also be attributed to an impact on the transfer function from the control voltage to the control force. The magnitude affects the control force, which corresponds to the control gain. The phase corresponds to the time-delay in the control system.

3. Influence Factors of Higher-Order CSI Effect

The influencing analysis of several factors, such as structural parametric uncertainties and control gains, on a higher-order CSI effect remain unknown. This section analyzes these influencing factors. Following this, several measures to reduce this effect can be obtained. A SDOF structure with an AMD system is intended to be a numerical example. Its parameters are listed in Table 2. Its Feedback gain G is calculated by an LQR algorithm, and the weight matrices Q and R are shown in Table 2.

Table 2. Parameters of the control system.

Structure			The AMD System			
Mass m (kg)	**Rigidity k (N/m)**	**Damping Ratio**	**AMD Mass m_a (kg)**	**AMD Rigidity k_a (N/m)**	Q	R
2×10^6	5×10^7	0.05	250	0.001	10^8	10^{-4}

3.1. Influence Analysis of Structural Parameters

The force equilibrium of a SDOF system can be described as:

$$m\ddot{x}(t) + c'\dot{x}(t) + k'x(t) = -u(t) + \ddot{x}_g(t) \tag{22}$$

where m, c', and k' are the nominal mass, damping, and stiffness of the SDOF system, respectively.

Since the uncertainties of structural damping or stiffness exist, the transfer functions of an AMD system from the control voltage to the control force can be obtained. The change in the stiffness and damping are described as:

$$k' = \beta k,\ c' = \alpha c\ (\alpha, \beta = 1, 2, \cdots, 5) \tag{23}$$

where β and α are the amplification factors of stiffness and damping, respectively.

Substituting Equation (23) into Equation (20) leads to:

$$\dot{\hat{Z}} = \begin{bmatrix} 0 & I & 0 \\ -\dfrac{\beta k}{m} & -\dfrac{\alpha c}{m} & \dfrac{1}{m} \\ 0 & \dfrac{K_b K_i K_g^2}{L_a r_m^2} B_s^T & -\dfrac{R_a}{L_a} \end{bmatrix} \hat{Z} + \begin{bmatrix} 0 & 0 \\ \dfrac{1}{m} & 0 \\ 0 & \dfrac{K_i K_g}{L_a r_m} \end{bmatrix} \begin{bmatrix} \ddot{x}_g \\ V \end{bmatrix} \tag{24}$$

Its observation equation is:

$$Y = \begin{bmatrix} I & 0 & 0 \\ 0 & I & 0 \\ -\dfrac{\beta k}{m} & -\dfrac{\alpha c}{m} & \dfrac{1}{m} \\ 0 & 0 & 1 \end{bmatrix} \hat{Z} + \begin{bmatrix} 0 & 0 \\ 0 & 0 \\ \dfrac{1}{m} & 0 \\ 0 & 0 \end{bmatrix} \begin{bmatrix} \ddot{x}_g \\ V \end{bmatrix} \tag{25}$$

The changes in the transfer functions from the control voltage to the control force of the AMD system with different stiffnesses and dampings are shown in Figures 9 and 10.

From Figure 9, with the increase of structural stiffness, its fundamental frequency becomes larger. When the frequency of the control voltage is consistent with the structural frequency, a sudden change in the transfer function is generated. Meanwhile, mutation positions gradually shift to the right side, which is shown in Figure 9a. Furthermore, as the frequency of the control voltage is smaller than the fundamental frequency, the system has a long time-delay (negative phase). Therefore, the chosen frequency should be greater than the fundamental structural frequency. For example, a suitable frequency of the control voltage of the experimental system is 10 Hz, which is larger than its fundamental frequency (0.162 Hz).

From Figure 10, because structural damping cannot change the structural fundamental frequency, the mutation positions of these transfer functions remain unchanged when the damping increases. Additionally, when the chosen frequency is greater than the fundamental frequency, the phase (negative value) of the transfer function becomes smaller with the increase in structural damping. This indicates that the CSI effect becomes more significant.

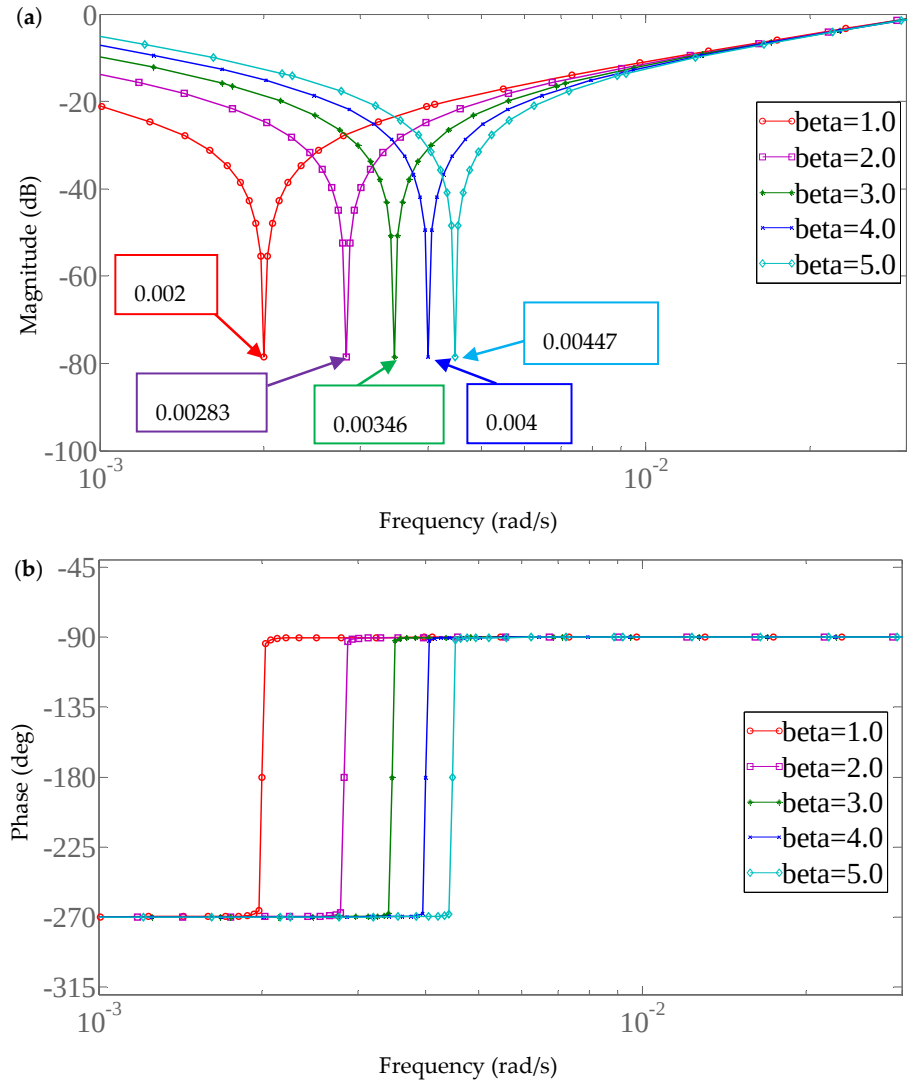

Figure 9. Transfer functions from control voltage to control force with different stiffnesses, (**a**) Magnitude; (**b**) Phase.

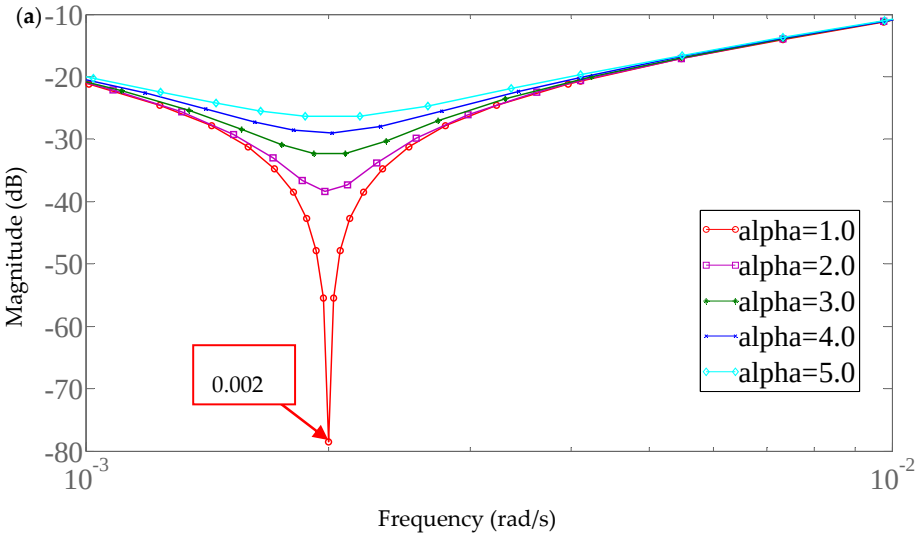

Figure 10. *Cont.*

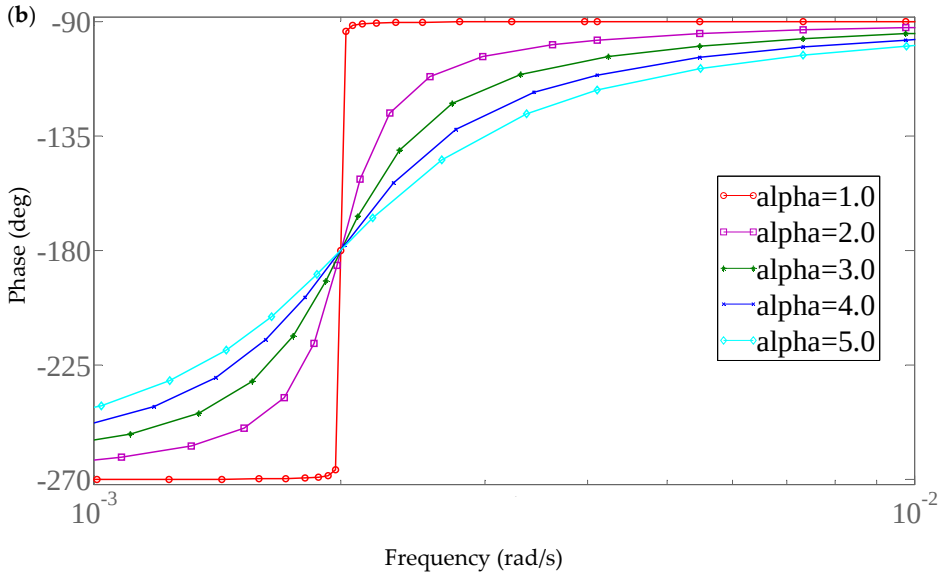

Figure 10. Transfer functions from control voltage to control force with different dampings, (**a**) Magnitude; (**b**) Phase.

3.2. Influence Analysis of Control Gains

The control force of a SDOF system is:

$$u = -\left(g_x x + g_{\dot{x}} \dot{x}\right) \tag{26}$$

where g_x and $g_{\dot{x}}$ are the control gain according to displacement and velocity, respectively.

The force equilibrium of a SDOF system can be described by substituting Equation (26) into Equation (22).

$$m\ddot{x}(t) + c\dot{x}(t) + kx(t) = -\left[g_x x(t) + g_{\dot{x}} \dot{x}(t)\right] + \ddot{x}_g(t) \tag{27}$$

Negative feedback control is commonly used in civil engineering, so two cases are analyzed for a SDOF system, namely:

$$g_x = \gamma k,\ g_{\dot{x}} = \varepsilon c\ (\gamma, \varepsilon = 1, 2, \cdots, 5) \tag{28}$$

When a higher-order CSI effect is considered, the state equation of the SDOF system is:

$$\dot{\hat{Z}} = \begin{bmatrix} 0 & I & 0 \\ -\frac{k}{m} & -\frac{c}{m} & \frac{1}{m} \\ \frac{R_a}{L_a} g_x & \frac{R_a}{L_a} g_{\dot{x}} + \frac{K_b K_i K_g^2}{L_a r_m^2} B_s^T & 0 \end{bmatrix} \hat{Z} + \begin{bmatrix} 0 & 0 \\ \frac{1}{m} & 0 \\ 0 & \frac{K_i K_g}{L_a r_m} \end{bmatrix} \begin{bmatrix} \ddot{x}_g \\ V \end{bmatrix} \tag{29}$$

Its observation equation is:

$$Y = \begin{bmatrix} I & 0 & 0 \\ 0 & I & 0 \\ -\frac{k}{m} & -\frac{c}{m} & \frac{1}{m} \\ 0 & 0 & 1 \end{bmatrix} \hat{Z} + \begin{bmatrix} 0 & 0 \\ 0 & 0 \\ \frac{1}{m} & 0 \\ 0 & 0 \end{bmatrix} \begin{bmatrix} \ddot{x}_g \\ V \end{bmatrix} \tag{30}$$

The changes of the phase transfer functions from the control voltage to the control force of the AMD system with different displacement and velocity gains are shown in Figures 11 and 12. From Figure 11, with the increase of the displacement gain, the absolute value of the phase

transfer function becomes smaller, which means that the time-delay of the system becomes shorter. From Figure 12, with the increase of the velocity gain (the equivalent damping of the system becomes larger), the absolute value of the phase transfer function becomes bigger, and indicating that the time-delay of the unstable system becomes longer.

In sum, system time-delay is inversely proportional to displacement gain, and is proportional to velocity gain. Therefore, for considering the stability of the system, when an algorithm is used in the design of a controller, it is necessary to guarantee that the weight coefficient according to displacement in the Q matrix is large and that the weight coefficient according to the velocity is small.

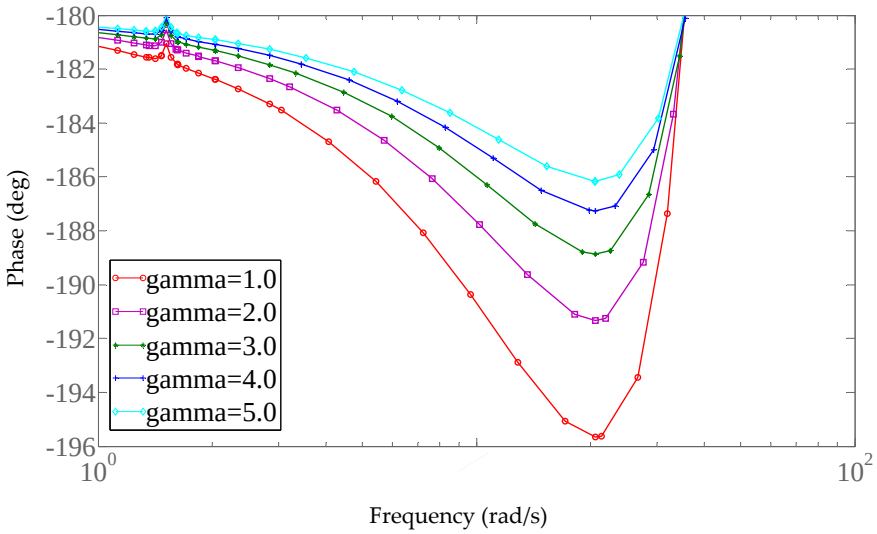

Figure 11. Phase transfer functions from control voltage to control force with different displacement gains.

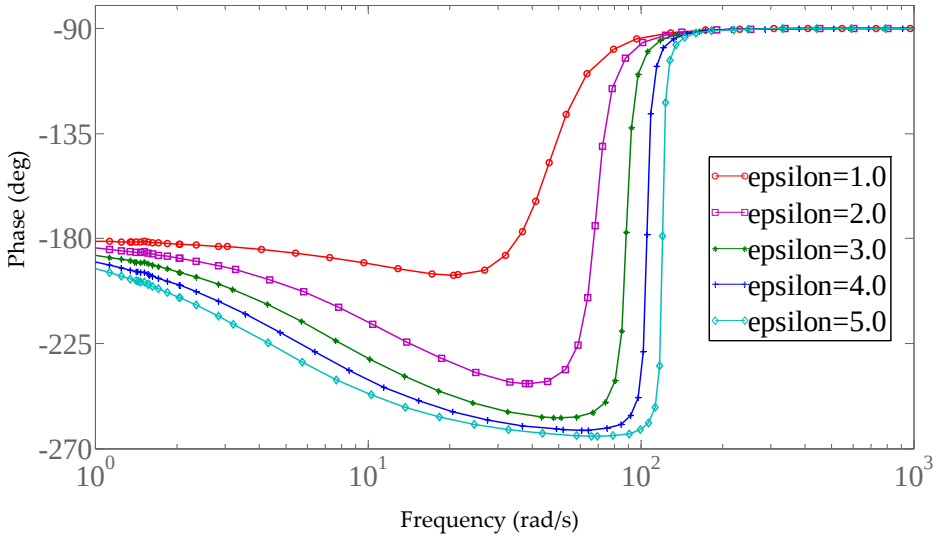

Figure 12. Phase transfer functions from control voltage to control force with different velocity gains.

4. Time-Delay Compensation Control Gain Design by GCC Algorithm

From Figures 7 and 8, when the frequency of the control voltage is determined, the phase from the input to output remains unchanged, meaning that the time-delay of the system is a certain value. However, as the frequency of the control voltage (affected by external excitation) is changed, the time-delay of the system is always changed. In this section, the time-delay resulted from a

higher-order CSI effect that can be calculated through numerical analysis. The process is coincident with the actual situation in civil engineering.

An El Centro seismic wave (SN direction) in Reference [19] is taken as an example. Three scenarios are analyzed for the seismic wave, namely: (1) Non-CSI effect; (2) Reduced-order CSI effect; and (3) Higher-order CSI effect. Using these systems, comparisons of control voltages and control forces are shown in Figure 13.

From Figure 13, under the excitation of the Centro El seismic wave, when the non-CSI effect and reduced-order CSI effect are considered, the control force and control voltage are basically in synchronization. Compared to the higher-order CSI effect, the time-delay between the control force and the control voltage is comparatively obvious, where the result is consistent with engineering practices.

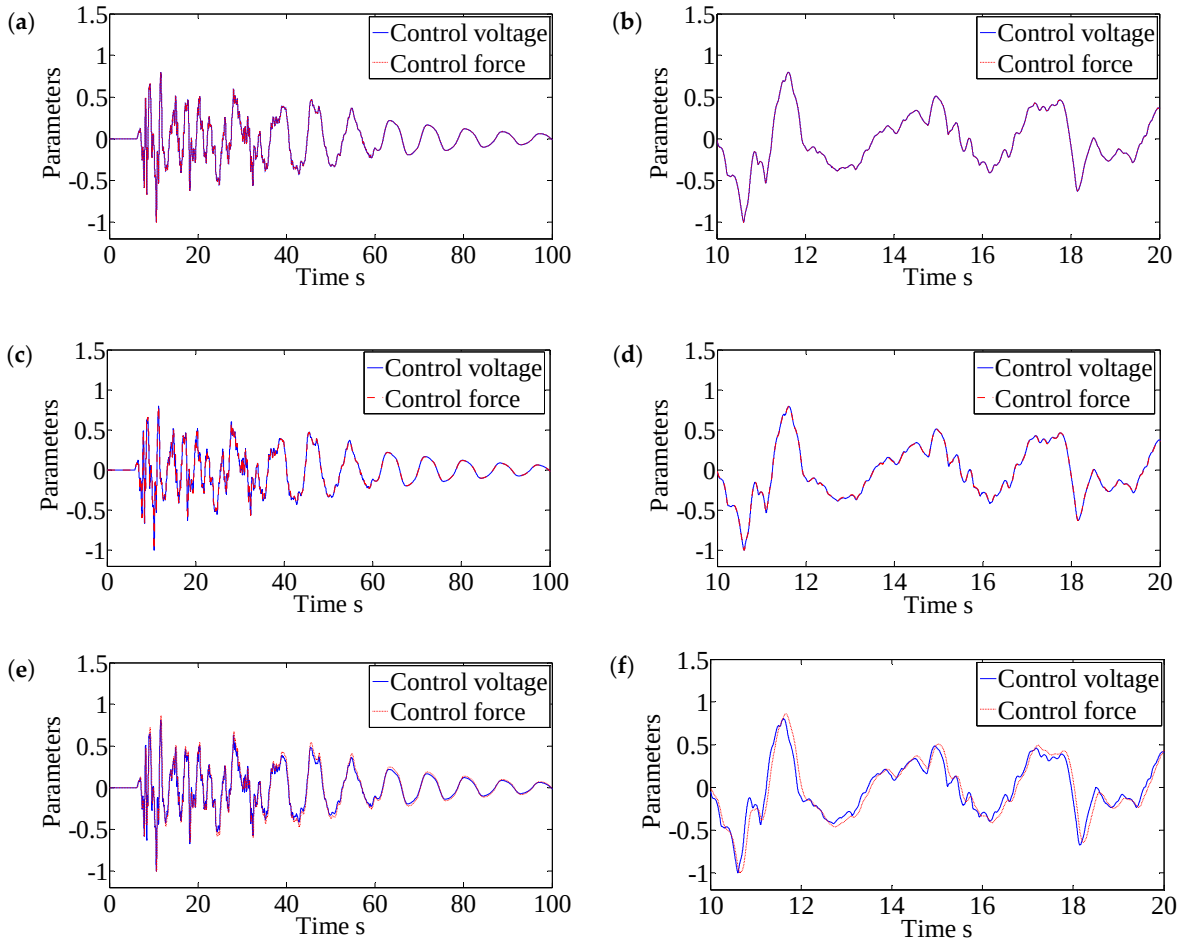

Figure 13. Control voltage and control force induced by the El Centro seismic wave, (**a**,**b**) Non-CSI effect; (**c**,**d**) Reduced-order CSI effect; (**e**,**f**) Higher-order CSI effect.

As the Higher-order CSI effect is considered, the time-varying delays of the experimental system are shown in Figure 14. From these figures, under the excitation of the El Centro seismic wave, the biggest time-delay is 0.11 s. Additionally, after the earthquake, the maximum time-delay (0.11 s) remains unchanged. As the excitation frequency (the frequency of control voltage) is zero, according to Figure 8, the phase is the largest, which means that this time-delay is the longest.

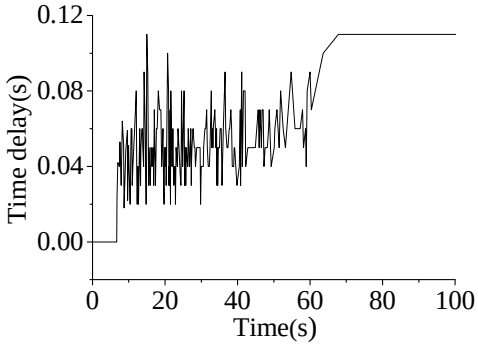

Figure 14. Time-varying delays of the experimental system.

Due to an external excitation with a changed frequency, the absolute velocity of the AMD mass is not zero and a higher-order CSI effect exists, which means that a time-varying delay also exists. The time-varying delay includes a constant part $d = (d_1 + d_2 + d_3 + d_4 + d_5)$ and a time-varying part $d_6(t)$.

The control force considering time-varying delay is:

$$u_d(t) = -GZ[t - d(t)] \tag{31}$$

where $d(t)$ is the time-varying delay.

Structural parameters M' and K', considering uncertainty, are:

$$M' = M + \Delta M = (1 + \delta_M)M,\ K' = K + \Delta K = (1 + \delta_K)K. \tag{32}$$

where δ_M and δ_K are the variation coefficients of the structural mass and stiffness, respectively.

The closed-loop system with uncertain parameters and a time-varying delay can be described as:

$$\dot{Z}(t) = (A + \Delta A)Z(t) + (B_2 + \Delta B_2)u_d(t) + (B_2 + \Delta B_2)u(t) \tag{33}$$

Supposing $\Delta\overline{A} = -\Delta\overline{B}_2 G$, system (33) is:

$$\dot{Z}(t) = (A + \Delta A)Z(t) + \left(\overline{A} + \Delta\overline{A}\right)Z[t - d(t)] + (B_2 + \Delta B_2)u(t) \tag{34}$$

The perturbation matrix is assumed follow the form described in Reference [33].

$$\begin{bmatrix} \Delta A & \Delta B_2 & \Delta\overline{A} \end{bmatrix} = DF\begin{bmatrix} E_1 & E_2 & E_d \end{bmatrix} \tag{35}$$

where F is an uncertain matrix satisfying $F = \overline{\delta}I$, $\left|\overline{\delta}\right| < 1$ and $\overline{\delta}$ is an uncertain constant. Moreover:

$$D = \begin{bmatrix} 0 & 0 \\ -\dfrac{K}{M} & -\dfrac{C}{M} \end{bmatrix},\ E_1 = \begin{bmatrix} \left[\dfrac{(\delta_K + 1)}{(\delta_M + 1)} - 1\right]I & 0 \\ 0 & \left[(\delta_M + 1)^{-1} - 1\right]I \end{bmatrix},\ E_2 = E_d = \begin{bmatrix} 0 \\ \dfrac{B_s\left[(\delta_M + 1)^{-1} - 1\right]}{C} \end{bmatrix}. \tag{36}$$

By substituting Equation (35) into Equation (34), and letting $u(t) = -G \cdot Z$, the state-equation of a control system is:

$$\dot{Z}(t) = [A - B_2 G + DF(E_1 - E_2 G)]Z(t) + \left(\overline{A} + DFE_d\right)Z(t - d) \tag{37}$$

The performance index of the system (37) can be defined as:

$$J = \int_0^\infty \left(Z^T QZ + U^T RU\right)dt = \int_0^\infty \left\{Z^T\left[Q + (-G)^T R(-G)\right]Z\right\}dt \tag{38}$$

Supposing $\widetilde{A} = A - B_2G + DF(E_1 - E_2G)$. If there exists symmetric positive-definite matrices $P, S \in R^{n\times n}$, then:

$$\begin{bmatrix} \widetilde{A}^TP + P\widetilde{A} + S + Q + (-G)^TR(-G) & P\left(\overline{A} + DFE_d\right) \\ \left(\overline{A} + DFE_d\right)^TP & -S \end{bmatrix} < 0 \tag{39}$$

Based on the Lyapunov stability theory [34], it proves that the system (37) is asymptotically stable. Defining:

$$Y = \begin{bmatrix} (A - B_2G)^TP + P(A - B_2G) + S + Q + (-G)^TR(-G) & P\overline{A} \\ \overline{A}^TP & -S \end{bmatrix} \tag{40}$$

Equation (39) can be written as:

$$Y + \begin{bmatrix} PD \\ 0 \end{bmatrix} F[(E_1 - E_2G) \quad E_d] + [(E_1 - E_2G) \quad E_d]^TF^T \begin{bmatrix} PD \\ 0 \end{bmatrix}^T < 0 \tag{41}$$

where the matrix F satisfies the condition $F^TF < I$.

If there exists a positive constant μ, inequality (41) can be written as:

$$Y + \mu \begin{bmatrix} PD \\ 0 \end{bmatrix} \begin{bmatrix} PD \\ 0 \end{bmatrix}^T + \mu^{-1}[(E_1 - E_2G) \quad E_d][(E_1 - E_2G) \quad E_d]^T < 0 \tag{42}$$

The proof can be found in Reference [35]. From Schur's complement [36], inequality (42) can be expressed as:

$$\begin{bmatrix} (A - B_2G)^TP + P(A - B_2G) + \mu PDD^TP + S + Q + (-G)^TR(-G) & P\overline{A} & (E_1 - E_2G)^T \\ \overline{A}^TP & -S & E_d^T \\ (E_1 - E_2G) & E_d & -\mu I \end{bmatrix} < 0 \tag{43}$$

Inequality (43) is pre and post multiplying diag$\{P^{-1}, I, I\}$, and defining $X = P^{-1}$:

$$\begin{bmatrix} H & \overline{A} & X(E_1 - E_2G)^T \\ \overline{A}^T & -S & E_d^T \\ (E_1 - E_2G)X & E_d & -\mu I \end{bmatrix} < 0 \tag{44}$$

where $H = X(A - B_2G)^T + (A - B_2G)X + \mu DD^T + XSX + X\left[Q + (-G)^TR(-G)\right]X$.

From Schur's complement, and defining $W = -GX$, inequality (44) can be described as:

$$\begin{bmatrix} \widetilde{H} & \overline{A} & (E_1X + E_2W)^T & X & W^T & X \\ \overline{A}^T & -S & E_d^T & 0 & 0 & 0 \\ E_1X + E_2W & E_d & -\mu I & 0 & 0 & 0 \\ X & 0 & 0 & -Q^{-1} & 0 & 0 \\ W & 0 & 0 & 0 & -R^{-1} & 0 \\ X & 0 & 0 & 0 & 0 & -S^{-1} \end{bmatrix} < 0 \tag{45}$$

where $\widetilde{H} = AX + B_2W + (AX + B_2W)^T + \mu DD^T$. Inequality (45) is pre and post multiplying diag$\{I, S^{-1}, I, I, I, I\}$, and defining $V = S^{-1}$, it can be expressed as:

$$\begin{bmatrix} \widetilde{H} & \overline{A}V & (E_1X + E_2W)^T & X & W^T & X \\ V\overline{A}^T & -V & VE_d^T & 0 & 0 & 0 \\ E_1X + E_2W & E_dV & -\mu I & 0 & 0 & 0 \\ X & 0 & 0 & -Q^{-1} & 0 & 0 \\ W & 0 & 0 & 0 & -R^{-1} & 0 \\ X & 0 & 0 & 0 & 0 & -V \end{bmatrix} < 0 \quad (46)$$

The LMI toolbox of Matlab can be used to solve the optimal solutions of μ', X', W', and V'. The state feedback control law for a time-delay system with parametric uncertainty is:

$$U = -GZ = W'(X')^{-1}Z \quad (47)$$

The GCC control gain shown in Equation (47) can be used to design a new compensation controller for AMD control systems with parametric uncertainties or time-varying delays caused by a higher-order CSI effect, which is different from those in the reference literature.

To validate the efficiency of the developed method, the compensation controller with a state feedback GCC algorithm is applied to the experimental system. This paper focuses on the displacement control effect of the 4th floor of the experimental system and the size of the AMD stroke. After adjusting, Q_4, Q_5, and R are taken as 6×10^6, 3×10^2, and 1×10^{-3}, respectively, and the weight coefficients of the other layers are all defined as one. Three scenarios are analyzed in this part: (1) The variation coefficients of the structure parameters are 0%, and the time-delay is zero; (2) The variation coefficients of the structure parameters are 0%, and the introduced time-varying delays are stochastic numbers (0 to 0.2 s); (3) The variation coefficients of stiffness and mass are −38.3% and 16.8%, and the introduced time-varying delays are stochastic numbers (0 to 0.2 s). The loading frequency and the peak value of the sinusoidal excitation force are 1 Hz and 45.89 N. Under the above excitation load, the control effects and the AMD parameters of different control systems are listed in Table 3, and the structural responses (includes displacement and acceleration) to the 4th floor of the different control systems are shown in Figures 15–17.

Table 3. Control effectiveness of structural responses.

Index		No Control	No Time-Delay		GCC Compensation		Uncertain System with GCC Compensation		
			Responses	Effect (%)	Responses	Effect (%)	No Control	Responses	Effect (%)
Displacement (m)	2nd floor	0.0298	0.0205	31.0591	0.0194	34.8642	0.0335	0.0219	34.7817
	3rd floor	0.0432	0.0295	31.7138	0.0277	35.8596	0.0491	0.0316	35.6275
	4th floor	0.0497	0.0338	31.9498	0.0320	35.6917	0.0563	0.0358	36.4951
Acceleration (m/s^2)	2nd floor	0.4028	0.1183	70.6267	0.1375	65.8645	0.4105	0.1332	67.5401
	3rd floor	0.3082	0.1001	67.5416	0.1172	61.9658	0.3501	0.1412	59.6573
	4th floor	0.3097	0.0756	75.5864	0.0875	71.7627	0.3426	0.0970	71.7008
AMD control forces (N)		–	27.8351	–	28.1549	–	–	28.3361	–
AMD strokes (m)		–	0.1635	–	0.1471	–	–	0.1873	–

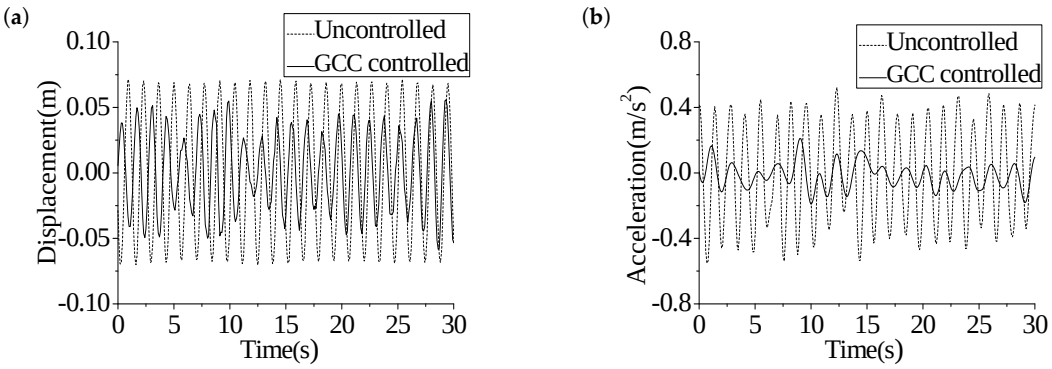

Figure 15. Comparison of structural responses to the 4th floor of the experimental system under scenario 1, (**a**) Displacement; (**b**) Acceleration.

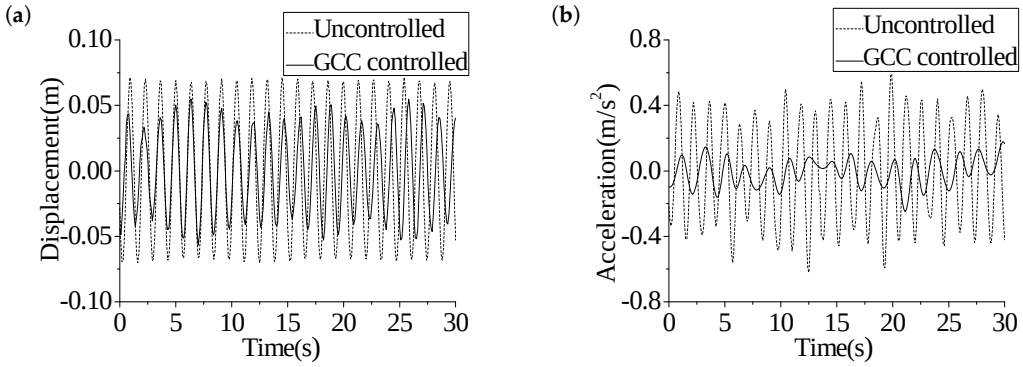

Figure 16. Comparison of structural responses to the 4th floor of the experimental system under scenario 2, (**a**) Displacement; (**b**) Acceleration.

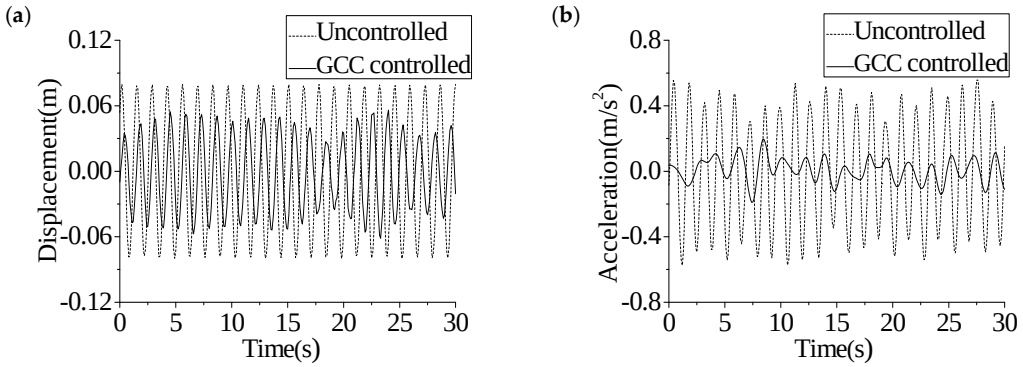

Figure 17. Comparison of structural responses to the 4th floor of the experimental system under scenario 3, (**a**) Displacement; (**b**) Acceleration.

From Figures 15–17 and Table 3, when the time-delay and the structural parametric uncertainty are not considered, the GCC controller can effectively suppress the structural response. Moreover, when considering the time-delay, the controller can also be used to compensate for the time-varying delay, and the maximum variations of the displacement and acceleration control effects between the systems with and without delays are only 4.15% and −5.58%, respectively. Additionally, as the structure parameters have a large uncertainty, the guaranteed cost controller is still valid. Compared with a certain system, the control effects of the displacement and acceleration responses of an uncertain system with GCC compensation only change by 0.80% and −2.31%, respectively.

Therefore, the guaranteed cost control method can effectively deal with the adverse conditions, and can be used to control the structural response in the ideal range.

5. Conclusions

The CSI effect has a negative influence in an AMD control system. To address this issue, three mathematical models of a four-storey steel frame are established, to consider the CSI effect in the paper. Several influence factors of a higher-order CSI effect are analyzed, including structural parameters and control gains. Finally, based on a GCC algorithm, the time-delay compensation controller is designed for the experimental system. Based on the results, the following conclusions can be drawn.

(1) As the CSI effect is discarded (Ideal situation), the magnitude of the transfer function is a constant, and the phase of the transfer function is zero, meaning that the transformation process does not contain a time-delay.
(2) When the CSI effect is considered, the above two parameters (magnitude and phase) are affected by the frequency of the control voltage, and the optimal frequency needs to approach the peak values of the magnitude and phase curves. As a result, a unit control voltage can be converted into a relatively large control force, and the additional time-delay is relatively short.
(3) The chosen frequency of the control voltage should be greater than the fundamental frequency of the controlled structure. At this time, the time-delay of control systems becomes longer, as the structural damping increases.
(4) The time-delay is inversely proportional to the displacement gain, and is proportional to the velocity gain. Therefore, it is necessary to guarantee that the weight coefficient according to displacement in the Q matrix is large and that the weight coefficient according to velocity is small.
(5) The time-delay of the system has time-varying characteristics. The controller based on the GCC algorithm in this paper can significantly improve the performance under the adverse influence of the time-varying delay, and its performance is close to the system without time-delay. As a result, it can effectively compensate for the time-delay and enhance the robustness of the control system with parametric uncertainties.

Acknowledgments: The research described in this paper was financially supported by the National Key Research and Development Program of China (Grant No. 2016YFC0701102), the National Natural Science Foundations of China (Grant No. 51378007 and 51538003), and the Shenzhen Technology Innovation Programs (Grant No. JSGG20150330103937411 and No. JCYJ20150625142543473).

Author Contributions: Chaojun Chen wrote the paper and summarized the results. Zuohua Li participated in the data analysis and conceived the study. Jun Teng and Ying Wang reviewed the study plan and corrected the grammatical mistakes.

Conflicts of Interest: The authors declare no conflict of interest.

References

1. Domaneschi, M.; Martinelli, L.; Po, E. Control of wind buffeting vibrations in a suspension bridge by TMD: Hybridization and robustness issues. *Comput. Struct.* **2015**, *155*, 3–17. [CrossRef]
2. Domaneschi, M.; Martinelli, L. Refined optimal passive control of buffeting-induced wind loading of a suspension bridge. *Wind Struct.* **2014**, *18*, 1–20. [CrossRef]
3. Spencer, B.F.; Nagarajaiah, S. State of the art of structural control. *J. Struct. Eng.* **2003**, *129*, 845–856. [CrossRef]
4. Teng, J.; Xing, H.B.; Xiao, Y.Q.; Liu, C.Y.; Li, H.; Ou, J.P. Design and implementation of AMD system for response control in tall buildings. *Smart Struct. Syst.* **2014**, *13*, 235–255. [CrossRef]
5. Basu, B.; Bursi, O.S.; Casciati, F.; Casciati, S.; Del Grosso, A.E.; Domaneschi, M.; Faravelli, L.; Holnicki-Szulc, J.; Irschik, H.; Krommer, M.; et al. A European Association for the Control of Structures joint perspective. Recent studies in civil structural control across Europe. *Struct. Control Health Monit.* **2014**, *21*, 1414–1436. [CrossRef]

6. Teng, J.; Xing, H.B.; Lu, W.; Li, Z.H.; Chen, C.J. Influence analysis of time delay to active mass damper control system using pole assignment method. *Mech. Syst. Signal Proccess.* **2016**, *80*, 99–116. [CrossRef]
7. Ou, J.P. *Active, Semi-Active and Intelligent Control in Civil Engineering Structure*; Science Press: Beijing, China, 2003.
8. Udwadia, F.E.; Phohomsiri, P. Active control of structures using time delayed positive feedback proportional control designs. *Struct. Control Health Monit.* **2006**, *13*, 536–552. [CrossRef]
9. Dong, Y.L.; Yang, F.W. Stability analysis and observer design for a class of nonlinear systems with multiple time-delays. *Adv. Differ. Equ.* **2013**, *2013*, 1–16. [CrossRef]
10. Dyke, S.J.; Spencer, B.F.; Quast, P.; Sain, M.K. Role of control-structure interaction in protective system-design. *J. Eng. Mech.* **1995**, *121*, 322–338. [CrossRef]
11. Battaini, M.; Yang, G.; Spencer, B.F. Bench-scale experiment for structural control. *J. Eng. Mech.* **2000**, *126*, 140–148. [CrossRef]
12. Ikeda, Y.; Sasaki, K.; Sakamoto, M.; Kobori, T. Active mass driver system as the first application of active structural control. *Earthq. Eng. Struct. Dyn.* **2001**, *30*, 1575–1595. [CrossRef]
13. Stewart, G.M.; Lackner, M.A. The effect of actuator dynamics on active structural control of offshore wind turbines. *Eng. Struct.* **2011**, *33*, 1807–1816. [CrossRef]
14. Spencer, B.F.; Sain, M.K. Controlling buildings: A new frontier in feedback. *IEEE Control Syst. Mag.* **1997**, *17*, 19–35. [CrossRef]
15. Soong, T.T.; Spencer, B.F. Supplemental energy dissipation: State-of-the-art and state-of-the practice. *Eng. Struct.* **2002**, *24*, 243–259. [CrossRef]
16. Liu, J.; Liu, H.J.; Dyke, S.J. Control-structure interaction for micro-vibration structural control. *Smart Struct. Syst.* **2012**, *21*, 52–53. [CrossRef]
17. Xing, J.T.; Xiong, Y.P.; Price, W.G. A generalised mathematical model and analysis for integrated multi-channel vibration structure-control interaction systems. *J. Sound Vib.* **2009**, *320*, 584–616. [CrossRef]
18. Messac, A.; Malek, K. Control structure integrated design. *AIAA J.* **2015**, *30*, 2124–2131. [CrossRef]
19. Zhang, C.W.; Ou, J.P. Control structure interaction of electromagnetic mass damper system for structural vibration control. *J. Eng. Mech.* **2008**, *134*, 428–437. [CrossRef]
20. Moreno, C.P.; Thomson, P. Design of an optimal tuned mass damper for a system with parametric uncertainty. *Ann. Oper. Res.* **2010**, *181*, 783–793. [CrossRef]
21. Wu, J.C.; Yang, J.N.; Schmitendorf, W.E. Reduced-order H∞ and LQR control for wind-excited tall buildings. *Eng. Struct.* **1998**, *20*, 222–236. [CrossRef]
22. Chen, Y.; Xue, A.K. Improved stability criterion for uncertain stochastic delay systems with nonlinear uncertainties. *Electron. Lett.* **2008**, *44*, 452–458. [CrossRef]
23. Boyd, S.; Ghaoui, L.E.; Feron, E.; Balakrishnan, V. *Linear Matrix Inequalities in System and Control Theory*; Society for Industrial and Applied Mathematics (SIAM): Philadelphia, PA, USA, 1994.
24. Pu, Z.L.; Rao, R.F. Delay-dependent LMI-based robust stability criterion for discrete and distributed time-delays Markovian jumping reaction-diffusion CGNNs under Neumann boundary value. *Neurocomputing* **2016**, *171*, 1367–1374. [CrossRef]
25. Mobayen, S. An LMI-based robust tracker for uncertain linear systems with multiple time-varying delays using optimal composite nonlinear feedback technique. *Nonlinear Dyn.* **2015**, *80*, 917–927. [CrossRef]
26. Ahmadi, A.; Aldeen, M. An LMI approach to the design of robust delay-dependent overlapping load frequency control of uncertain power systems. *Int. J. Electr. Power Energy Syst.* **2016**, *81*, 48–63. [CrossRef]
27. Kim, K.H.; Park, M.J.; Kwon, O.M.; Lee, S.M.; Cha, E.J. Stability and robust H∞ control for time-delayed systems with parameter uncertainties and stochastic disturbances. *J. Electr. Eng. Technol.* **2016**, *11*, 200–214. [CrossRef]
28. Chang, S.; Peng, T. Adaptive guaranteed cost control of systems with uncertain parameters. *IEEE Trans. Autom. Control* **1972**, *17*, 474–483. [CrossRef]
29. Gyurkovics, E. Guaranteed cost control of discrete-time uncertain systems with both state and input delays. *Int. J. Control* **2016**, *89*, 2073–2082. [CrossRef]
30. Cheres, E.; Palmor, Z.J.; Gutman, S. Quantitative measures of robustness for systems including delayed perturbations. *IEEE Trans. Autom. Control* **1989**, *34*, 1203–1204. [CrossRef]
31. Moheimani, S.; Petersen, I.R. Optimal quadratic guaranteed cost control of a class of uncertain time-delay systems. *IEE Proc. Control Theory Appl.* **1997**, *144*, 183–188. [CrossRef]

32. Guo, S.X. Robust reliability method for non-fragile guaranteed cost control of parametric uncertain systems. *Syst. Control Lett.* **2014**, *64*, 27–35. [CrossRef]
33. Khargonekar, P.P.; Petersen, I.R.; Zhou, K.M. Robust stabilization of uncertain linear-systems-quadratic stabilizability and H∞ control theory. *IEEE Trans. Autom. Control* **1990**, *35*, 356–361.
34. Sastry, S. *Lyapunov Stability Theory*; Springer: New York, NY, USA, 1999.
35. Xie, L.H. Output feedback H∞ control of systems with parameter uncertainty. *Int. J. Control* **1996**, *63*, 741–750. [CrossRef]
36. Zhang, F. *The Schur Complement and Its Applications*; Springer: Berlin, Germany, 2005.